fishes

Article

Spatiotemporal Distribution of Antarctic Silverfish in the Ross Sea, Antarctica

Sara Lee [1], Wooseok Oh [2], Hyoung Sul La [3], Wuju Son [3,4], Jeong-Hoon Kim [5] and Kyounghoon Lee [6,*]

1 Department of Fisheries Physics, Pukyong National University, Busan 48513, Republic of Korea; wogurtlfgdj@naver.com
2 Institute of Low-Carbon Marine Production Technology, Pukyong National University, Busan 48513, Republic of Korea; owsnice@gmail.com
3 Division of Ocean & Atmosphere Sciences, Korea Polar Research Institute, Incheon 21990, Republic of Korea; hsla@kopri.re.kr (H.S.L.); swj5753@kopri.re.kr (W.S.)
4 Department of Polar Sciences, University of Science and Technology, Daejeon 34113, Republic of Korea
5 Division of Life Sciences, Korea Polar Research Institute, Incheon 21990, Republic of Korea
6 Division of Marine Production System Management, Pukyong National University, Busan 48513, Republic of Korea
* Correspondence: klee71@pknu.ac.kr; Tel.: +82-51-629-5889; Fax: +82-51-629-5886

Abstract: Antarctic silverfish (*Pleuragramma antarcticum*) play a crucial intermediary role in connecting top predators and krill in the food web of the Antarctic Ocean. Despite their crucial role, research on their abundance is lacking. In this study, we estimated the abundance of juvenile Antarctic silverfish as foundational data for predicting their abundance. The density of juvenile Antarctic silverfish was estimated using an acoustic backscattering theoretical model. The mean volume backscattering strength was used to investigate the vertical and horizontal distributions of juvenile Antarctic silverfish in the Antarctic Ross Sea. The survey area was located near Cape Hallett, Antarctica, where Antarctic krill (*Euphausia superba*), ice krill (*E. crystallorophias*), and Antarctic silverfish coexist. The survey was performed four times using the Korean Antarctic research ship, RV Araon (R/V, 7507 GT). Frame trawls were conducted to identify the length and weight of the target fish species in the survey area. Captured Antarctic silverfish captured measured 3–9 cm. The maximum target strength (TS) was −92.93 dB at 38 kHz, −86.63 dB at 120 kHz, and 85.89 dB at 200 kHz. The average TS was −100.00 dB at 38 kHz, −93.00 dB at 120 kHz, and −106.90 dB at 200 kHz. Most juvenile Antarctic silverfish were found at a depth of 100 m and were distributed closer to sea ice. Between nearshore and polynya waters, the fish demonstrated a proclivity for polynya waters.

Keywords: Antarctic silverfish; hydroacoustic; mean volume backscattering strength

Key Contribution: Antarctic silverfish play a crucial intermediary role in the food web of the Antarctic ecosystem, making it a highly important species. Assessing the resources of Antarctic silverfish is vital, particularly using underwater acoustics as a technique. Target strength (TS) is a crucial factor in evaluating resources through acoustics, and we estimated the TS of Antarctic silverfish, elucidating their spatiotemporal distribution. This paper contributes to a better understanding of the Antarctic ecosystem.

check for updates

Citation: Lee, S.; Oh, W.; La, H.S.; Son, W.; Kim, J.-H.; Lee, K. Spatiotemporal Distribution of Antarctic Silverfish in the Ross Sea, Antarctica. *Fishes* **2024**, *9*, 47. https://doi.org/10.3390/fishes9020047

Academic Editors: Jianfeng Tong, Yong Tang and Tohru Mukai

Received: 15 December 2023
Revised: 20 January 2024
Accepted: 23 January 2024
Published: 26 January 2024

1. Introduction

Antarctic silverfish (*Pleuragramma antarcticum*) is an important fish species in the Antarctic Ross Sea owing to its wide distribution and high abundance, serving as prey for both marine mammals and birds [1]. It also plays an important role in the food chain of the Ross Sea by feeding on Antarctic krill (*Euphausia superba*), linking top predators to krill [2–4]. Therefore, Antarctic silverfish have a significant impact on the abundance of top predators and krill in the Antarctic.

Antarctic silverfish is the only notothenioid species with an entire pelagic life cycle [5]. It also has a larval stage of more than one year, which is longer than that of other fish species. The larvae are initially distributed in surface waters, and as they mature, they disperse into deeper waters [6,7].

Antarctic silverfish can be classified into three age groups based on their length [3,8,9]. Specimens between 0.8 and 3 cm in length are classified as post-larvae, and those between 3 and 10 cm in length as juvenile fish. Specimens larger than 11 cm in length are classified as adult fish. Juvenile Antarctic silverfish is highly abundant in Antarctic waters, accounting for 98% of the total plankton [10].

The abundance of a target species is generally predicted based on the abundance of its juveniles. Therefore, estimating the abundance of juvenile Antarctic silverfish is a crucial factor in predicting the overall abundance of Antarctic silverfish.

Among various methods used to determine the density and distribution of organisms, the hydroacoustic technique is the most effective method for surveying waters with limited access and time limits, like those in Antarctica. To extract echo signals from the target fish species using the hydroacoustic technique, it is important to discern the target strength (TS) of the target fish species. The acoustic scattering model is most commonly used to measure the TS of fish species, as this model takes into account several variables, such as size, swimming angle, size of the swimbladder, and usage frequency, as well as morphological characteristics of the target fish species. In the acoustic scattering theoretical model (Kirchhoff–Ray mode), TS can be estimated by calculating the sum of the volumes of the fish body and swimbladder, approximated as cylindrical shapes. This theoretical model is a method of estimating acoustic backscatter strength by separating specific anatomical structures of the target species, which is generally more precise than estimating strength using only the organism's shape [11].

Abundance estimation of a target species using acoustic techniques can be calculated by dividing the volume backscattering strength (Sv) collected in the field by the target strength (TS) of the target species. However, given the diversity of species in the ocean, it is essential to first identify the target species and then separate their signals for accurate analysis. There are two methods for separating the signals of the target species: time-varied threshold (TVT), which uses one frequency, and mean volume backscattering strength (MVBS), which uses more than two frequencies [12].

In this study, we measured the TS of juvenile Antarctic silverfish using an acoustic backscattering theoretical model to estimate the spatiotemporal distribution of juvenile Antarctic silverfish. We utilized MVBS to determine the vertical and horizontal distributions of juvenile Antarctic silverfish in the Antarctic Ross Sea. We believe this study can provide foundational data for predicting the abundance of Antarctic silverfish.

2. Materials and Methods

2.1. Survey Regions and Acoustic Data Collection

The study area was in the waters near Cape Hallet, Antarctica, where Antarctic krill (*E. superba*), ice krill (*E. crystallorophias*), and Antarctic silverfish coexist. Furthermore, the survey area is a known nursery ground for Antarctic silverfish [13]. The survey was conducted four times: from 16 February to 10 March 2018; 21 December 2018 to 18 January 2019; 3 March to 7 April 2020; and 6 December to 22 December 2020 (Table 1). The acoustic transects in each survey were 6, 12, 12, and 10, respectively. The Korean Antarctic research ship, the icebreaker RV Araon (R/V, 7507 G/T), was used for the survey. Acoustic data were collected while maintaining a vessel speed of 7–10 knots (Figures 1 and 2).

Table 1. Survey period.

Survey Rounds	Survey Period	Survey Transects
1st	16 February 2018–10 March 2018	06
2nd	21 December 2018–18 January 2019	12
3rd	3 March 2020–7 April 2020	12
4th	6 December 2020–22 December 2020	10

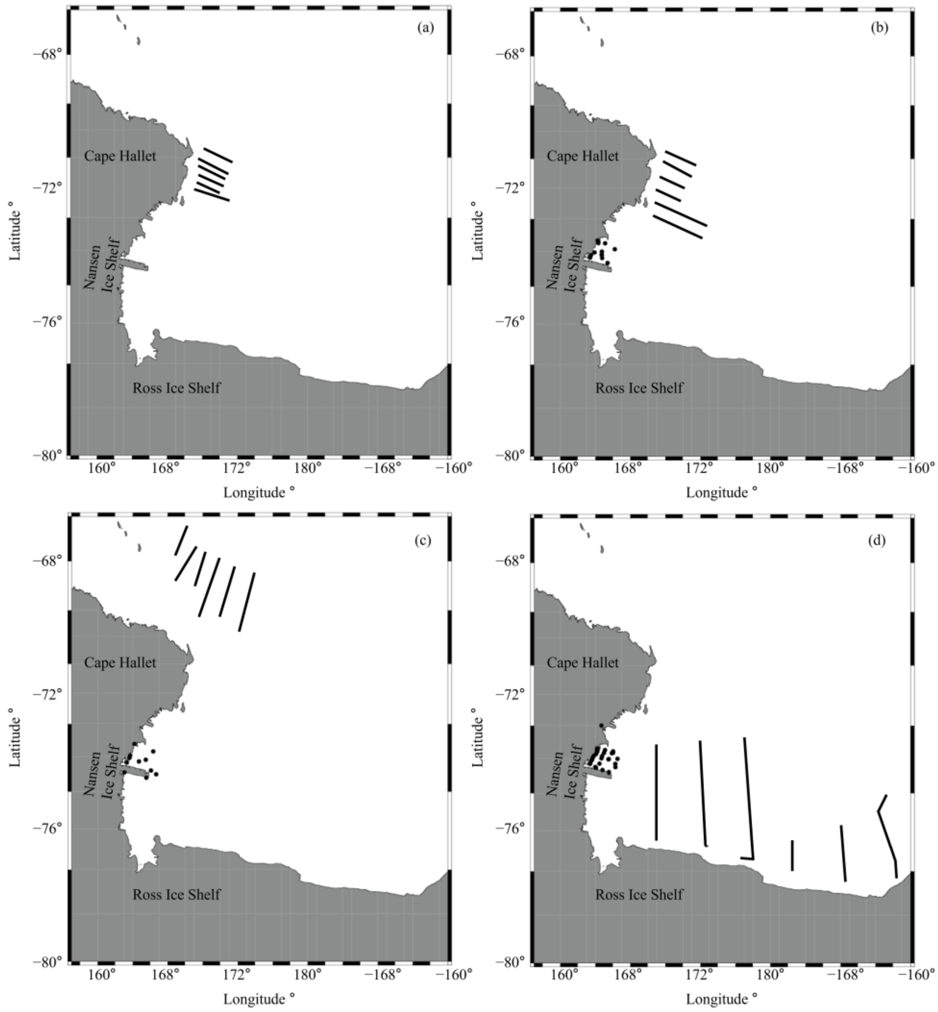

Figure 1. Location map of the acoustic survey transects in the Ross Sea. (**a**) February 2018, (**b**) December 2018, (**c**) March 2020, and (**d**) December 2020. The black dots represent icons generated for drawing lines, while the lines symbolize acoustic survey transects.

2.2. Sample Catch Data

It was necessary to determine the length and weight of the target fish species to evaluate species density via hydroacoustics. Therefore, quantitative fishing gear to collect the target fish species in the survey area was required. Since the shape of the net structure changes depending on the speed of the survey vessel, a small midwater trawl with a frame trawl of 2 m $\times$ 2 m was used. The frame was made of stainless steel with a diameter of 100 mm. For stable fishing gear deployment, five buoys were installed on the top for buoyancy, and four 100 kg weights were attached to the lower bar for reinforcing weight and stability (Figure 3). The net was manufactured in duplicate by using double-walled nets of approximately 7 m; the outer net protected the inner net from breakage. The mesh sizes of the inner and outer nets were 5 and 10 mm, respectively. The square frame net was used as fishing gear to collect fish larvae and specimens.

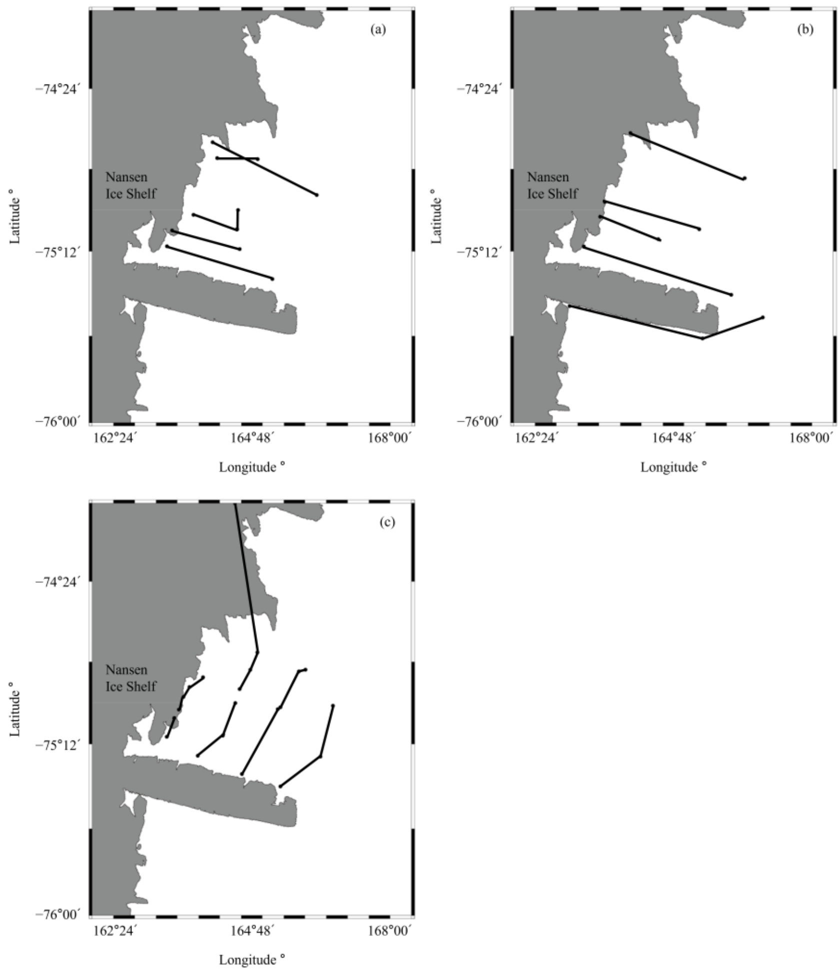

Figure 2. Location map of the acoustic survey transects in polynya waters. (**a**) December 2018, (**b**) March 2020, and (**c**) December 2020.

Figure 3. Frame midwater trawl and attached buoys.

Collections via the frame trawl were carried out on the Ross Sea ice shelf, located offshore of the continental shelf in relatively shallow water with a depth ranging from 600 to 700 m [14]. A total of eight voyages were carried out between 7 and 16 December 2020 (Figure 4). While maintaining a vessel speed of 2–3 knots, the net was towed for more than 30 min, and acoustic data were collected simultaneously.

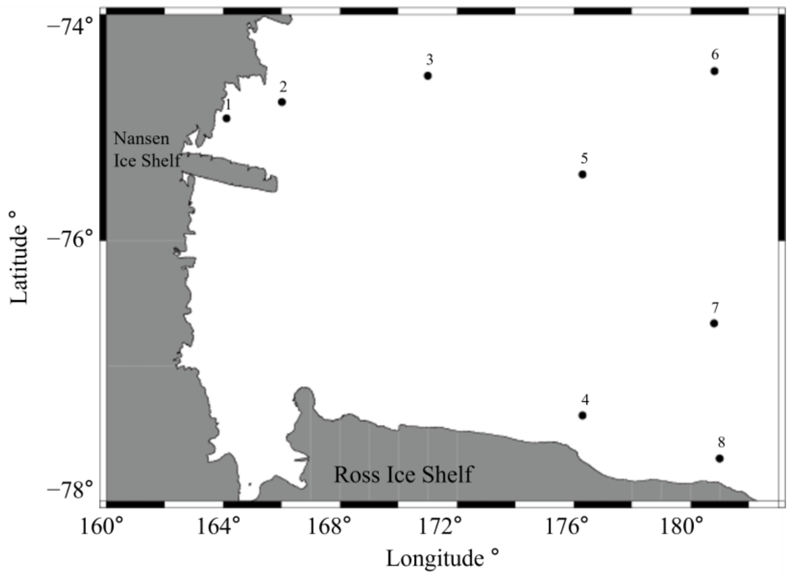

Figure 4. Location map of the frame midwater trawl stations conducted in the Ross Sea.

2.3. The Kirchhoff–Ray Mode (KRM)

The Kirchhoff–Ray mode (KRM) model was applied to estimate the acoustic scattering intensity of Antarctic silverfish in the Antarctic Ross Sea. The KRM model (Equations (1) and (2)) can identify and quantify the shape of the fish body to estimate acoustic scattering strength [15].

$$L_{FISH} = L_{BODY} = f(f_r, \theta_{tilt}, S_b, \rho_w, \rho_b, c_w, c_b) \tag{1}$$

$$TS = 10\log_{10}|L_{FISH}|^2 \tag{2}$$

where f_r is the frequency, θ_{tilt} is the angle between the body axis and the incidence angle, S_b is the body shape of the fish approximated as a cone, ρ_w is the density of the medium (seawater), ρ_b is the density of the fish body, c_w is the velocity of sound of the medium (seawater), and c_b is the velocity of sound of the fish body.

The TS using the KRM model calculates the posture angle from $-60°$ to $60°$ at $1°$ intervals. The maximum and average values of TS were evaluated; the average values (Equations (3) and (4)) were calculated using the probability density function (PDF), while assuming an average posture angle and standard deviation of $-5°$ and $15°$, respectively, for common fish. The TS of each posture angle calculated every $1°$ was replaced by the scattering cross-section, multiplied by the PDF of the posture angle of $-5 \pm 15°$, and then the average TS was calculated using the sum [16]:

$$\sigma_{bs} = \int_{-\pi/2}^{\pi/2} \sigma(\theta) f(\theta) d\theta \tag{3}$$

$$TS_{avg.} = 10\log_{10}\sigma_{avg.} \tag{4}$$

where *σ(θ)* is the backscattering cross-section at each swimming angle θ, and *f(θ)* refers to the frequency of occurrence of each swimming angle. Additionally, the *TS* relation for Antarctic silverfish can be expressed by Equations (5) and (6). Equation (6) assumes that the reflection intensity is proportional to the second power of the length:

$$TS = a\log_{10} L + b \tag{5}$$

$$TS = 20log_{10}L + TS_{10} \tag{6}$$

where *a* is a slope, *b* is an intercept, and *L* indicates length (cm).

The KRM model estimates acoustic scattering strength by calculating the sum of the approximate volumes of the fish body and the swimbladder. However, in the case of

Antarctic silverfish, the formula for the swimbladder was removed when applying the model, as this species does not have a swimbladder [13]. For the density and sound velocity ratios of the target species, this study utilized the findings of a previous study, which were 1.012 and 1.015, respectively [17].

Since contour data are required to use the KRM model, photographs were taken by enumerating Antarctic silverfish. The pictures of the samples were analyzed using a digitizing software program (Getdata Ver. 2.26, https://getdata-graph-digitizer.software.informer.com; accessed on 14 December 2023) to collect body shape coordinates by dividing the sides of the fish body into 0.2 mm intervals. This information was applied in the KRM model.

2.4. Data Processing

Acoustic data acquired through a scientific echosounder often include various acoustic noises, leading to the degradation of the normal echo signal. The noise in the acoustic data of this study included background, transient, and impulse noises (Figure 5). Background noise occurs when the survey depth is out of the detection range of the used frequency, and the acoustic intensity is relatively strong. Noise was removed by considering the values of the data samples in the horizontal and vertical ranges. Background noise was removed by converting the value of the data sample to −999 dB if the signal-to-noise ratio (*SNR*) value was greater than the threshold value(δ) when artificial noise was subtracted from the data sample in the specified area; this method is called TVT (Table 2). The *SNR* at the ping (i) and range sample (j) is defined as follows:

$$SNR(i,\ j) = S_{v,\ corr}(i,j) - S_{noise}(i,j)$$

$$if\ SNR(i,\ j)\ \leq\ threshold_{SNR'} \tag{7}$$

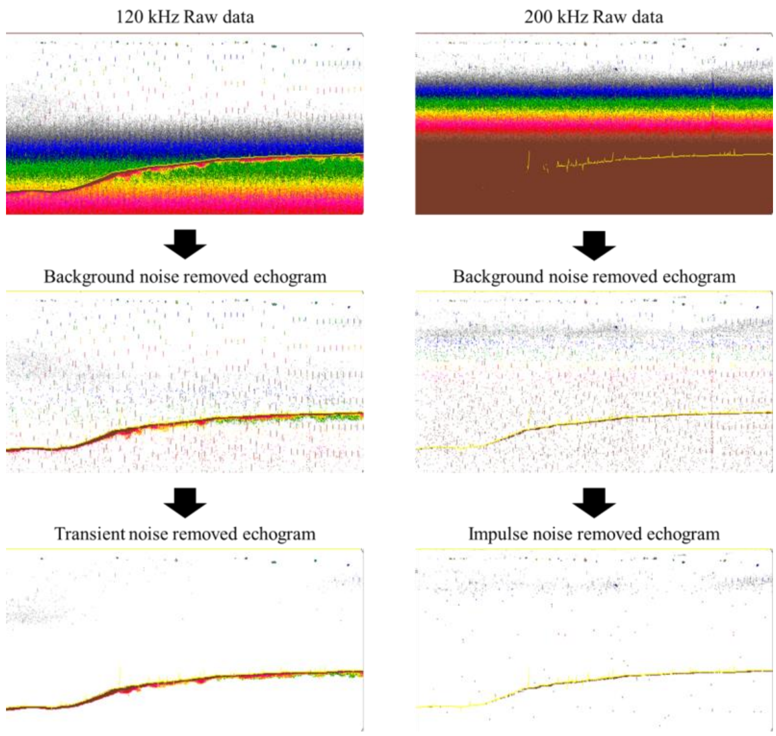

Figure 5. Examples of noise processing in the echogram. The intensity is indicated by the color, with red representing high intensity and blue indicating low intensity.

Table 2. Background noise parameters.

Frequency	120 kHz	200 kHz
Horizontal extent (ping)	20	20
Vertical units	samples	samples
Vertical extent (samples)	5	5
Vertical overlap (%)	0	0
Maximum noise (dB)	−125	−250
Minimum SNR	10	10

Transient noise is electrical noise caused by various on-board electrical equipment and is characterized by a regular drizzling pattern [18]. Transient noise was removed as follows: when a range of ~7 pings in the horizontal direction of the data sample was set, and the median value of the area was subtracted from the center data sample in the specified area, the noise was removed if the value was greater than the threshold value (Table 3).

$$S_{vi,j} - \overset{\sim}{S_{vm,n}} > \delta. \tag{8}$$

Table 3. Transient noise parameters.

Frequency	120 kHz
Exclude above	Fixed depth surface exclusion at 10 m
Exclude below	Minimum integration stop depth
Exclude below threshold (dB at 1 m)	−170
Vertical window units	Samples
Vertical window size (samples)	5
Horizontal size (ping)	7
Vertical size (samples)	9
Calculations per sample	63
Percentile	50
Threshold (dB)	10
Noise sample replacement value	Percentile
percentile	10

Impulse noise occurs due to interferences from acoustic equipment installed on other ships and is characterized by irregular, thick rain patterns. Impulse noise was removed using the following process: after each sample value of the horizontal range variations was subtracted from the central data sample of the specified area, a value was obtained. If the value was greater than the threshold value, the noise was removed; this method is called the two-sided comparison method (Table 4).

$$S_{vi,j} - S_{v(i+n),\quad j} > \delta and$$

$$S_{vi,j} - S_{v(i-n),\quad j} > \delta \tag{9}$$

Table 4. Impulse noise parameters.

Frequency	200 kHz
Exclude above	Surface
Exclude below	Bottom
Exclude below threshold (dB at 1 m)	−150
Vertical window units	Samples
Vertical window size (samples)	3
Horizontal size (pings)	3
Threshold (dB)	10
Noise sample replacement value	Mean

The frequency difference was the difference in the MVBS. The acoustic backscatter strength of the target species was extracted to obtain a positive value; low frequencies were subtracted from high frequencies. The acoustic scattering strength of the scatter predicted by the KRM model was calculated to be −92.69 dB at 120 kHz and −90.46 dB at 200 kHz when considering the minimum length (3 cm), and −69.95 dB at 120 kHz and −70.72 dB at 200 kHz when considering the maximum length (9 cm). Therefore, the $MVBS_{200kHz-120kHz}$ range of Antarctic silverfish in the echograms of the two frequencies received from the same seawater volume was from 2.23 to −0.77 dB. The frequency difference was applied to the results of the collections in December 2020. The acoustic backscatter strength of Antarctic silverfish was greater at 200 kHz than at 120 kHz.

To calculate the $MVBS_{200kHz-120kHz}$ within the same seawater volume after removing the noise from the sea surface and seafloor, the cell size (width × length) per frequency was applied to 1 ping × 1 m and integrated to generate a new echogram. A data range bitmap that set the frequency difference range of Antarctic silverfish was created. A mask operator was used to separate the echo signal from Antarctic silverfish by superimposing the echoes that matched the cell size with 120 kHz frequency at 200 kHz. Matched echoes were considered to be fish.

To estimate the density of juvenile Antarctic silverfish using acoustics, volume backscattering strength (Sv) data extracted from the scientific echosounder at 1 n.mile intervals were converted to nautical area scattering coefficients ($NASC$s). The relationship for converting Sv to $NASC$ can be found in Equation (10):

$$NASC = 4\pi 1852^2 \int_{r_1}^{r_2} Svdr \tag{10}$$

Since the $NASC$ value is the linear sum of the signals received from aquatic organisms in the water volume, the density of the target organisms (ρ, g/m^2) can be calculated by dividing the average $NASC$ value in the obtained seawater volume by the TS of the target fish; the TS and backscattering cross-section according to the length (L, mm) of the target organisms can be expressed in Equations (12) and (13), respectively:

$$NASC = \rho \cdot TS \tag{11}$$

$$TS = 20log(L) + TS_{mm} \tag{12}$$

$$\sigma = 4\pi 10^{\frac{TS}{10}} \tag{13}$$

Additionally, the length (L, mm)–weight (w, mg) relationship of the target organism can be found in Equation (14):

$$\omega = \alpha L^b \tag{14}$$

Here, the backscattering cross-section and length–weight function of the target organism were obtained from the catch data collected at the same time as the acoustic survey. The density of the target species (ρ) (Equation (15)) can be calculated by dividing the average $NASC$ within the seawater volume at 1 n.mile intervals by the backscattering cross-section (σ) of the target species and multiplying it by its weight. The remainder on the right side of Equation (15), except for $NASC$, is the conversion factor (CF) that calculates density from acoustic data, considering the backscattering cross-section and length–weight of the target species. Average values were utilized for the backscattering cross-section and weight of the target species.

$$\rho = \left(\frac{NASC}{\sigma}\right) \cdot \omega = \frac{\alpha L^b}{4\pi 10^{TS/10}} \cdot NASC \tag{15}$$

The average target species density ($\overline{\rho}$) of the entire survey area represents the weighted mean of the average density data per vessel, as shown in Equation (16):

$$\overline{\rho} = \frac{\sum_{i=1}^{N} \overline{\rho} \cdot n_i}{\sum_{i=1}^{N} n_i} \tag{16}$$

where $\overline{\rho}_i$ is the mean density of the ith vessel, n_i is the number of the ith vessel (elementary distance sampling unit, EDSU), and N indicates the number of vessels.

3. Results

A distribution survey of Antarctic silverfish was performed using a frame trawl in the Antarctic Ross Sea in December 2020. The individuals captured in the fishing gear were juvenile Antarctic silverfish. Antarctic silverfish were most abundantly caught at station 5, with a total of 46 individuals. (Table 5). The catch ratio of Antarctic silverfish was >53% at station 1 (Figure 6). The variation in the lengths of the fish obtained using the fishing gear is shown in Figure 6. Antarctic silverfish caught had a length of 3–9 cm. Fish with a 5 cm body length were found in the highest proportion, accounting for approximately 53% of the captured fish, whereas 6 cm fish were captured in the lowest proportion (Figure 7).

Table 5. Trawl time, station, location, number caught, and catch rate.

Station	Date (DD.MM.YYYY)	Latitude (°)	Longitude (°)	Number Caught (N)	Antarctic Silverfish Ratio (% by Number)
1	12.07.2020	74°56.9′ S	164°06.8′ E	15	53.3 333 3
2	12.09.2020	74°48.2′ S	166°00.4′ E	106	
3	12.11.2020	74°34.0′ S	171°00.1′ E	123	15.4
4	13.12.2020	77°22.4′ S	176°17.9′ E	155	1.3
5	14.12.2020	75°26.4′ S	176°17.9′ E	150	30.7
6	14.12.2020	74°31.5′ S	179°11.0′ W	103	1.0
7	15.12.2020	76°40.0′ S	179°11.9′ W	7	14.3
8	16.12.2020	77°41.6′ S	179°00.3′ W	28	21.4

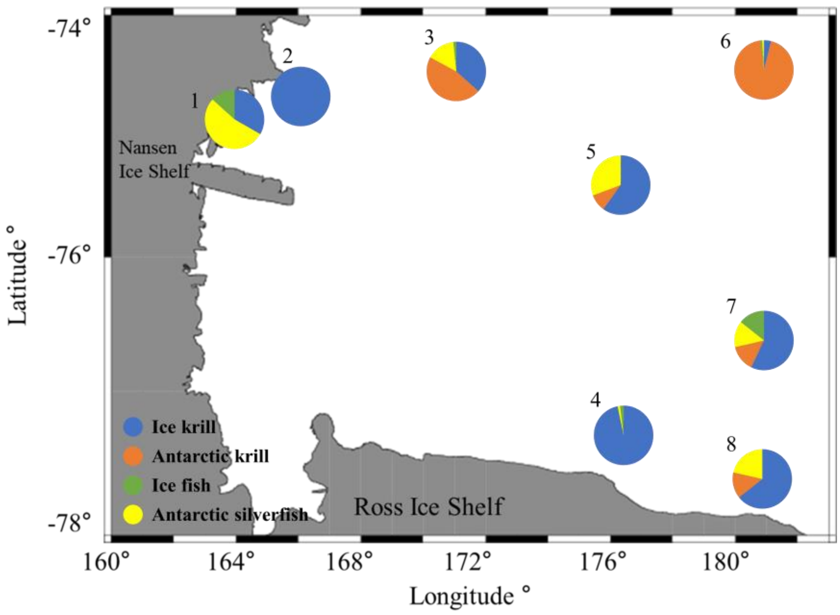

Figure 6. Distribution of caught species according to trawl station.

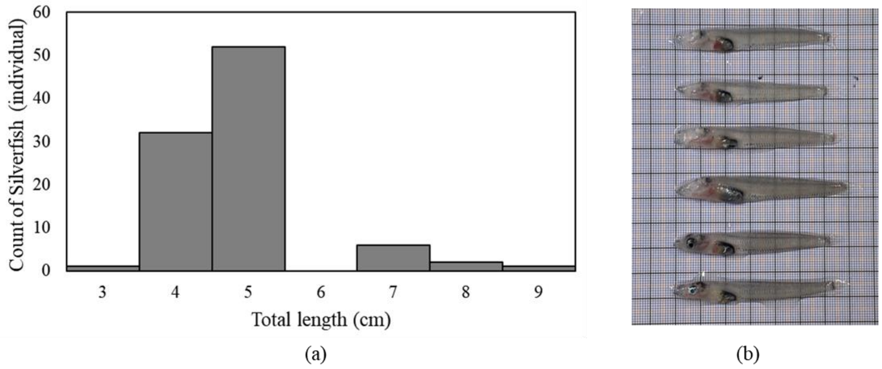

Figure 7. Antarctic silverfish sampled in December 2020 using frame midwater trawl. (**a**) Total length distribution. (**b**) Photograph of sampled Antarctic silverfish.

The maximum TS of Antarctic silverfish, calculated from the theoretical model of hydroacoustic scattering in line with their variation in posture angle [−45° to +45°], refers to the highest value between such posture angles of −45° to 45°; the average TS is the value calculated using PDF for a posture angle of −5 ± 15° [16]. The relationship between the total length and maximum TS of Antarctic silverfish was as follows:

$TS = 52.13\log_{10} TL - 119.00$ at 38 kHz,
$TS = 52.10\log_{10} TL - 112.67$ at 120 kHz
And $TS = 46.32\log_{10} TL - 107.24$ at 200 kHz

The relationship between the total length and average TS was as follows:

$TS = 47.74\log_{10} TL - 118.44$ at 38 kHz,
$TS = 47.65\log_{10} TL - 115.43$ at 120 kHz
And $TS = 41.37\log_{10} TL - 110.21$ at 200 kHz

The maximum TS of the reference TS, which was calculated with the frequency-specific TS proportional to the second power of length, was −92.93 dB at 38 kHz, −86.63 dB at 120 kHz, and −85.89 dB at 200 kHz; the average TS of Antarctic silverfish was −100.00 dB at 38 kHz, −93.00 dB at 120 kHz, and −106.90 dB at 200 kHz.

The vertical distribution of the NASC values for Antarctic silverfish in the nearshore waters of the Antarctic Ross Sea is shown in Figure 8. The detection range at a frequency of 200 kHz was considered in 10 m intervals from a depth of 15 m to a depth of 155 m. The vertical distribution in February 2018 showed low NASC values in all water layers. The vertical distribution in December 2018 showed the highest value of 4.29 m^2/nm^2 at a depth of 25 m. The NASC values in March 2020 were highest at the surface with 8.3 m^2/nm^2, but NASC values lowered with increasing depth. The values in December 2020 were highest at the surface, and higher values were found at depths of 50 and 60 m. Most high NASC values were found within 20 m. The vertical distribution of NASC values of the Antarctic silverfish in the polynya area in the Antarctic Ross Sea was as follows: strong NASC values were found at the surface in December 2018; in March 2020, NASC values tended to increase with depth. NASC values in December 2020 were found to be high at a depth of 20 m and higher at depths of 50 and 80 m. Both nearshore and polynya waters showed a strong distribution at the surface.

The horizontal distribution of the fish is shown in Figures 8 and 9, where the color of the circle indicates the size of the NASC (Figures 9 and 10). In February 2018, NASC values in the Ross Sea were generally low in intensity. The NASC values for juvenile Antarctic silverfish in the Ross Sea in December 2018 were stronger near the sea ice, and the strongest intensity was found near −75° latitude and 172° longitude. The NASC values for juvenile Antarctic silverfish in the Ross Sea in March 2020 were generally low, similar to the values in December 2018. The horizontal distribution of juvenile Antarctic silverfish in the Ross Sea in December 2020 was mostly even, and a strong intensity was found between −74° and −75° latitude. The distribution of juvenile Antarctic silverfish was stronger in December compared with February and March. The horizontal distribution of juvenile Antarctic silverfish in the polynya waters in December 2018 was found to be mostly low, with higher intensity in the north of the survey area. In March 2020, the horizontal distribution of juvenile Antarctic silverfish in the polynya waters was largely in the north of the Drygalski Trough, located at −75° latitude and 163–164° longitude. In December 2020, the horizontal distribution of juvenile Antarctic silverfish in the polynya waters showed a strong intensity near −78° latitude and 168–176° longitude, while the average NASC of the fish species per vessel was generally even.

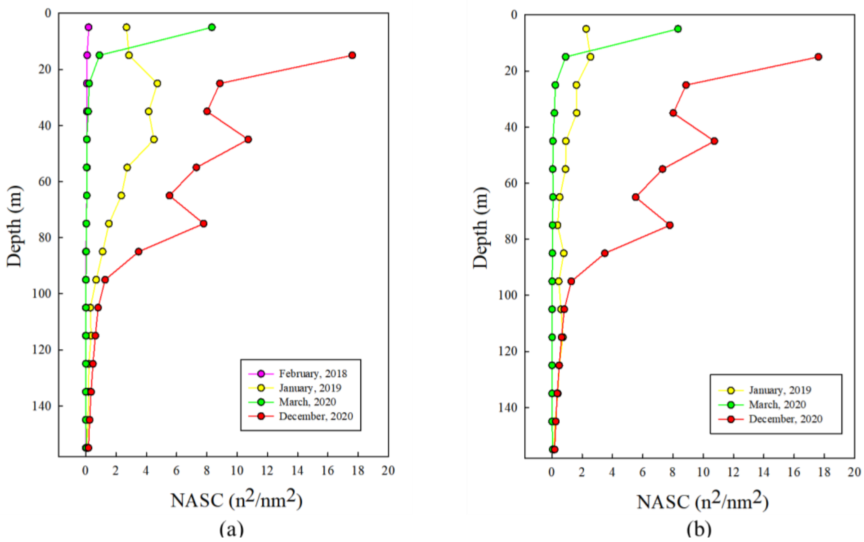

Figure 8. Vertical distribution of Antarctic silverfish NASC values. (**a**) Ross Sea and (**b**) polynya waters.

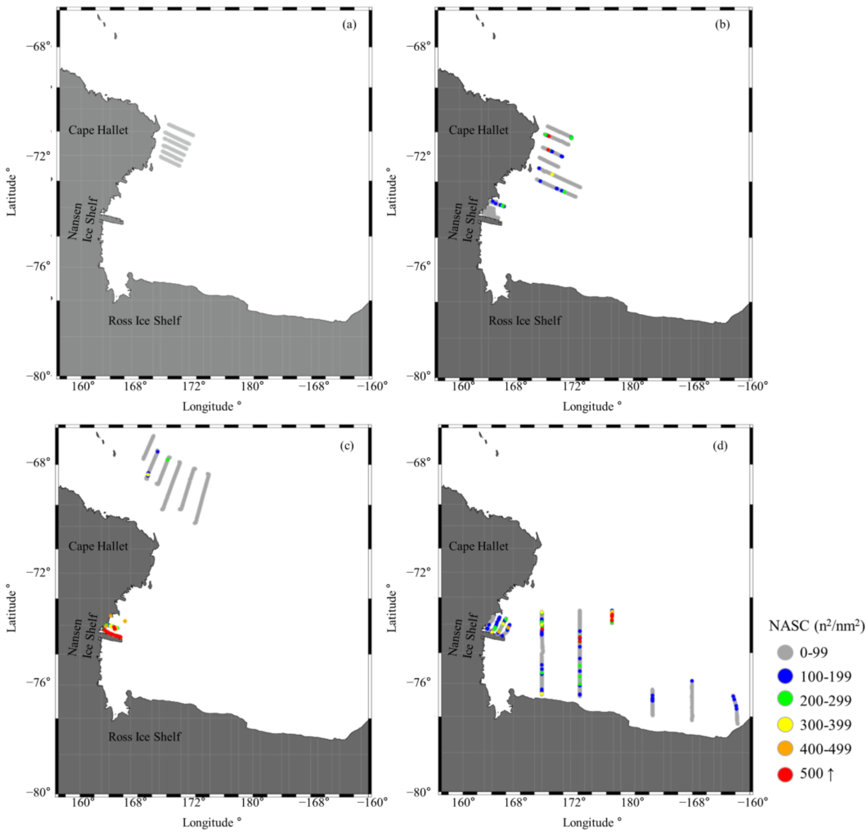

Figure 9. Horizontal distribution of Antarctic silverfish NASC values in the Ross Sea. (**a**) February 2018, (**b**) December 2018, (**c**) March 2020, and (**d**) December 2020.

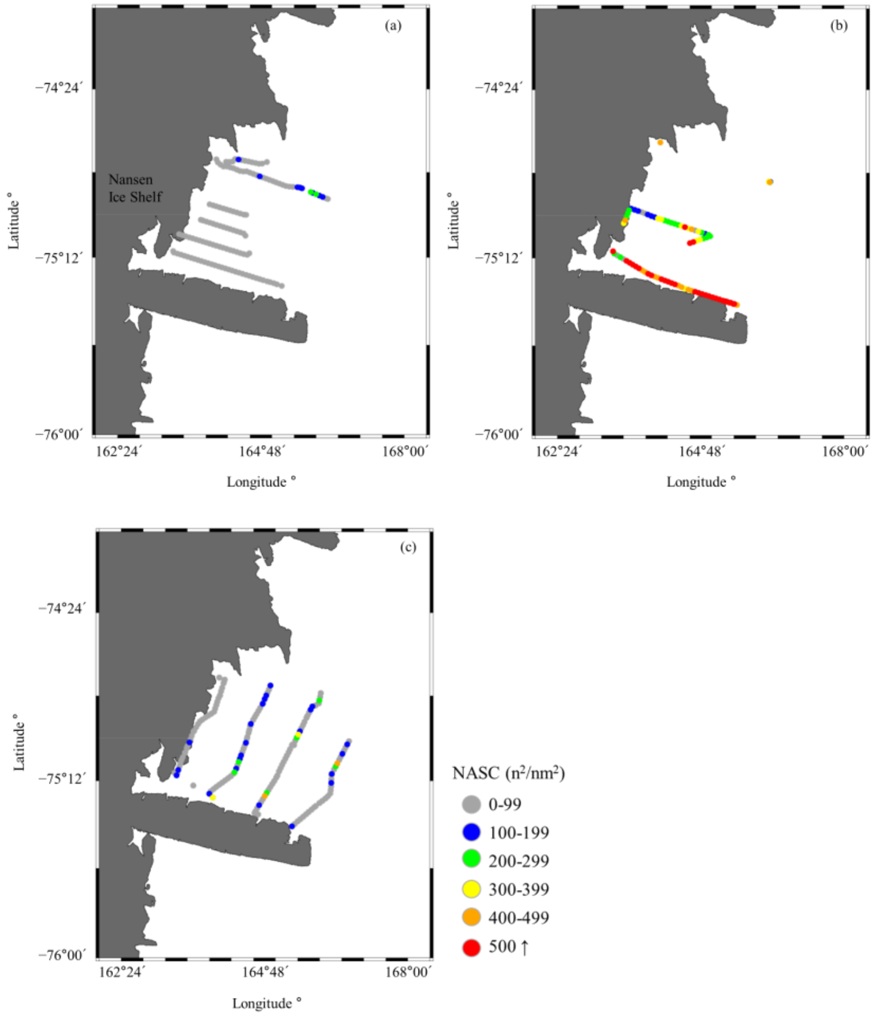

Figure 10. Horizontal distribution of Antarctic silverfish NASC values in polynya waters. (**a**) December 2018, (**b**) March 2020, and (**c**) December 2020.

In February 2018, the average density of the fish species in the nearshore waters of the Antarctic Ross Sea was 0.004 (g/m^2). In December 2018, the average density of the fish species was 0.058 (g/m^2) in the nearshore waters of the Antarctic Ross Sea and 0.008 (g/m^2) in the polynya waters. In March 2020, the average density of the fish species in the Antarctic Ross Sea was 0.029 (g/m^2) in the nearshore waters and 1.468 (g/m^2) in the polynya waters, confirming that the density was 50 times higher in the polynya waters than in the nearshore waters. In December 2020, the average density of the fish species in the Antarctic Ross Sea was 0.269 (g/m^2) in the nearshore waters and 0.337 (g/m^2) in the polynya waters. Higher densities were found in the polynya waters compared with nearshore waters, except in December 2018.

4. Discussion

Based on the same length, juvenile Antarctic silverfish have similar acoustic backscatter strength to Antarctic krill and show similar primary distribution depths to ice krill [19]. The current study examined post-larval Antarctic silverfish of 3–10 cm in length. The lengths of the collected krill were substantially different from those of Antarctic silverfish, and the acoustic scattering strengths were therefore also assumed to differ substantially (Table 6).

Table 6. Length distribution of Antarctic krill, ice krill, and Antarctic silverfish, sampled in December 2022.

	Antarctic Krill (*Euphausia superba*)	Ice Krill (*Euphausia crystallorophias*)	Antarctic Silverfish (*Pleuragramma antarcticum*)
Minimum length (cm)	3.14	1.77	3.42
Maximum length (cm)	4.95	3.92	9.40
Average length (cm)	4.10	2.79	4.83
Standard deviation	3.24	4.51	0.96

By comparing the MVBS (200–120 kHz) difference in the range 3–5 cm, where the lengths overlapped, the difference of MVBS (200–120 kHz) between Antarctic silverfish and Antarctic krill (*E. superba*) became similar as the lengths increased (Figure 11). Therefore, future studies should be conducted on the acoustic backscatter strength of Antarctic silverfish, Antarctic krill, and ice krill to develop algorithms that can more clearly distinguish the three species. Additionally, krill are characterized by large-scale clustering, whereas juvenile Antarctic silverfish tend to be more dispersed [20,21]. Therefore, studies of their clustering or dispersion patterns may also be helpful in distinguishing them.

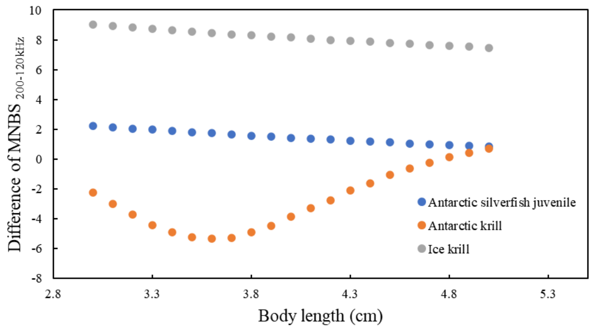

Figure 11. Comparison of the MVBS (200–120 kHz) values in the range of 3–5 cm among Antarctic silverfish, Antarctic krill, and ice krill.

The fishing gear used in the December 2018 survey was a frame trawl, which is designed to prevent the net from being damaged by vessel speed and currents. The length of Antarctic silverfish caught in this survey was 3–9 cm. Unlike previous studies focusing on post-larval and adult Antarctic silverfish, this study only targeted juvenile fish [22]. However, it was not easy to handle large sampling equipment, such as frame trawls, and move to target depths in Antarctic waters [23]. In the future, frame trawls may need to be equipped with real-time monitoring depth sensors to determine depth movements.

In a previous study by La Mesa et al. [3] that targeted Antarctic silverfish and estimated acoustic scattering intensities, the fish were divided into adult fish and larvae to estimate the acoustic scattering features; however, as the sample size employed in the current study corresponds to the size classified as fish larvae in the previous study, only acoustic scattering features of fish larvae were compared. In previous studies, the body shape of Antarctic silverfish is described as a spherical shape based on body depth, and the current study extended this into a cylindrical shape for body depth and width. The ratio of body width to depth of the Antarctic silverfish was approximately 0.08; since body width is relatively small, we assumed that there would be a large difference in acoustic scattering intensities. A previous study and the present study showed that acoustic scattering intensities increased in line with higher frequencies, which is a feature of fish species without a swimbladder [21].

O'Driscoll et al. [21] indicated that adult Antarctic silverfish are mainly distributed at depths of 100–400 m, whereas juvenile fish are mainly distributed in shallow waters at a depth of 80 m. Since echo signals were identified by applying the acoustic backscatter strength of juvenile Antarctic silverfish in the current study, we assumed that the echo signals did not appear in deeper waters.

Vacchi et al. [10] showed that Antarctic silverfish spawn near sea ice. In the present study, a large number of fertilized eggs of Antarctic silverfish were found near Terra Nova, the survey area. Antarctic silverfish were found to be distributed near sea ice. The phenomenon is speculated to be due to the fact that this research was conducted during the Antarctic summer when Antarctic silverfish is attracted by the influx of phytoplankton caused by warmer temperatures and melting sea ice.

Polynya is a geographical term indicating an ice-free area in polar oceans where sea ice is present and remains ice-free almost all year round. In this area, the biomass growth and primary production of phytoplankton increase due to the restrictions from physical phenomena such as wind, glaciers, and heat. In the survey area, the Terra Nova Bay polynya and the Ross Ice Shelf polynya are formed, which may explain the high distribution of Antarctic silverfish near polynya. Furthermore, both the Ross Ice Shelf polynya and Terra Nova Bay polynya are reported to produce the maximum amount of sea ice in March [24], which may explain the high fish distribution near the polynya in March 2020. In other survey periods, such as February and December 2018, the sea ice area in the Antarctic Ross Sea was the least developed of the corresponding months from 1981 to 2010 [25]. In particular, the sea ice rarely developed in February compared with December, which may explain the low density of Antarctic silverfish due to less development in its spawning ground.

5. Conclusions

In this study, the vertical and horizontal distribution of juvenile Antarctic silverfish was investigated using the MVBS method. The study area encompassed regions where Antarctic silverfish coexist with Antarctic krill and ice krill. The frequency range applied was based on the estimated acoustic backscattering strength of Antarctic silverfish using the KRM. The analysis of the acoustic backscattering strength of juvenile Antarctic silverfish using the KRM model revealed that as the frequency increased, the TS also increased. For species like Antarctic silverfish, which lack swimbladders, the swimming angle is an essential variable influencing TS. However, research on the swimming angle of juvenile Antarctic silverfish is currently limited. Therefore, it is essential to investigate the swimming angle of Antarctic silverfish schools in the future. The spatiotemporal distribution results indicate that they predominantly inhabit the upper 80 m of the water column, with higher intensity observed near ice-covered areas. Antarctic silverfish is a species known to spawn near ice, suggesting a need for specific research on the relationship between Antarctic silverfish and sea ice in the future. This study estimated the TS of Antarctic silverfish, and it confirmed that the difference in MVBS between Antarctic krill and ice krill is distinct. Despite these differences, the echogram analysis still occasionally misidentified krill as Antarctic silverfish. However, the distribution patterns of Antarctic silverfish and krill were markedly different. Consistent with the findings of the previous study, this study similarly reveals that krill forms schools, while juvenile Antarctic silverfish exhibit a dispersed distribution pattern [21]. Although an analyst can manually exclude krill based on these patterns, problems arise due to notable variations in results depending on the analyst. Therefore, it is necessary to develop algorithms for the precise determination of Antarctic silverfish distribution patterns in the future. We believe this study can offer foundational data on the abundance of juvenile Antarctic silverfish.

Author Contributions: Conceptualization, S.L. and K.L.; methodology, S.L.; software, W.O.; validation, H.S.L., J.-H.K. and W.S.; formal analysis, S.L.; investigation, W.O., H.S.L. and W.S.; resources, K.L.; data curation, S.L. and W.O.; writing—original draft preparation, S.L.; writing—review and editing, S.L.; visualization, S.L.; supervision, K.L.; project administration, K.L.; funding acquisition, H.S.L. and J.-H.K. All authors have read and agreed to the published version of the manuscript.

Funding: This research was supported by the Korea Institute of Marine Science & Technology Promotion (KIMST) funded by the Ministry of Oceans and Fisheries (KIMST-20220547).

Institutional Review Board Statement: Ethics Committee: CNU laboratory animal research center. Approval code: CNU IACUC-YS-2021-8. Approval date: 28 October 2021.

Data Availability Statement: No new data were created or analyzed in this study. Data sharing is not applicable to this article.

Acknowledgments: We acknowledge the support and dedication of the captain and crew of IBRV ARAON for completing the field work with positive energy. We would like to thank Euna Yoon and Hyungbeen Lee for providing valuable advice on the analysis of the KRM model. Finally, we are grateful to Sunyoung Oh and Geunchang Park for providing valuable advice, counsel, and guidance.

Conflicts of Interest: The authors declare no conflicts of interest.

References

1. Corso, A.D.; Steinberg, D.K.; Stammerjohn, S.E.; Hilton, E.J. Climate drives long-term change in Antarctic Silverfish along the western Antarctic Peninsula. *Commun. Biol.* **2022**, *5*, 104. [CrossRef]
2. La Mesa, M.; Eastma, J.T.; Vacchi, M. The role of notothenioid fish in the food web of the Ross Sea shelf waters: A review. *Polar Biol.* **2004**, *27*, 321–338. [CrossRef]
3. La Mesa, M.; Catalano, B.; Russo, A.; Greco, S.; Vacchi, M.; Azzali, M. Influence of environmental conditions on spatial distribution and abundance of early life stages of Antarctic silverfish, *Pleuragramma antarcticum* (Nototheniidae), in the Ross Sea. *Antarct. Sci.* **2010**, *22*, 243–254. [CrossRef]
4. Sutton, C.P.; Horn, P.L. A preliminary assessment of age and growth of Antarctic silverfish. *CCAMLR Sci.* **2011**, *18*, 75–86.
5. Tavernier, E.; Giraldo, C. Trophic ecology of early developmental stages of Antarctic silverfish. In *The Antarctic Silverfish: A Keystone Species in a Changing Ecosystem*; Springer: Berlin/Heidelberg, Germany, 2017; pp. 113–130.
6. Gon, O.; Heemstra, P.C. *Fishes of the Southern Ocean*; JBL Smith Institute of Ichthyology: Grahamstown, South Africa, 1990; pp. 313–316. [CrossRef]
7. Giraldo, C.; Cherel, Y.; Vallet, C.; Mayzaud, P.; Tavernier, E.; Moteki, M.; Koubbi, P. Ontogenic changes in the feeding ecology of the early life stages of the Antarctic silverfish (*Pleuragramma antarcticum*) documented by stable isotopes and diet analysis in the Dumont d'Urville Sea (East Antarctica). *Polar Sci.* **2011**, *5*, 252–263. [CrossRef]
8. Hubold, G. Stomach contents of the Antarctic silverfish *Pleuragramma antarcticum* from the southern and eastern Weddell Sea (Antarctica). *Polar Biol.* **1985**, *5*, 43–48. [CrossRef]
9. Koubbi, P.; O'Brien, C.; Loots, C. Spatial distribution and inter-annual variations in the size frequency distribution and abundances of *Pleuragramma antarcticum* larvae in the Dumont d'Urville Sea from 2004 to 2010. *Polar Sci.* **2011**, *5*, 225–238. [CrossRef]
10. Vacchi, M.; La Mesa, M.; Dalu, M.; MacDonald, J. Early life stages in the life cycle of Antarctic silverfish, *Pleuragramma antarcticum* in Terra Nova Bay, Ross Sea. *Antarct. Sci.* **2004**, *16*, 299–305. [CrossRef]
11. Park, G.C.; Oh, W.S.; Oh, S.Y.; Lee, K.H. Acoustic scattering characteristics of chub mackerel (*Scomber japonicus*) by KRM model. *J. Korean Soc. Fish. Ocean Technol.* **2022**, *58*, 32–38. [CrossRef]
12. Do, M.A.; Surti, A.M. Estimation of dorsal aspect target strength of deep-water fish using a simple model of swimbladder backscattering. *J. Acoust. Soc. Am.* **1990**, *87*, 1588–1596. [CrossRef]
13. Vacchi, M.; Bottaro, M.; DeVries, A.L. A nursery area for the Antarctic silverfish *Pleuragramma antarcticum* at Terra Nova Bay (Ross Sea): First estimate of distribution and abundance of eggs and larvae under the seasonal sea-ice. *Polar Biol.* **2012**, *35*, 1573–1585. [CrossRef]
14. Yoon, S.T. Responses of the Ross Sea to the climate change: Importance of observations in the Ross Sea, Antarctica. *Ocean Polar Res.* **2022**, *44*, 69–82. [CrossRef]
15. Foote, K.G.; Traynor, J.J. Comparison of walleye pollock target strength estimates determined from in situ measurements and calculations based on swimbladder form. *J. Acoust. Soc. Am.* **1988**, *83*, 9–17. [CrossRef]
16. Hwang, K.S.; Lee, K.H.; Hwang, B.K. Verification and application of Target Strength for Japanese anchovy (*Engraulis japonicas*) by theoretical acoustic scattering model. *J. Korean Soc. Fish. Ocean Technol.* **2012**, *48*, 487–494. [CrossRef]
17. Azzali, M.; Leonori, I.; Biagiotti, I.; De Felice, A.; Angiolillo, M.; Bottaro, M.; Vacchi, M. Target strength studies on Antarctic silverfish (*Pleuragramma antarcticum*) in the Ross Sea. *CCAMLR Sci.* **2010**, *17*, 75–104.
18. Ryan, T.E.; Downie, R.A.; Kloser, R.J.; Keith, G. Reducing bias due to noise and attenuation in open-ocean echo integration data. *ICES J. Mar. Sci.* **2015**, *72*, 2482–2493. [CrossRef]
19. La, H.S.; Lee, H.; Kang, D.; Lee, S.; Shin, H.C. Ex situ echo sounder target strengths of ice krill *Euphausia crystallorophias*. *Chin. J. Oceanol. Limnol.* **2015**, *33*, 802–808. [CrossRef]
20. Tarling, G.A.; Klevjer, T.; Fielding, S.; Watkins, J.; Atkinson, A.; Murphy, E.; Leaper, R. Variability and predictability of Antarctic krill swarm structure. *Deep Sea Res. Part I Oceanogr. Res. Pap.* **2009**, *56*, 1994–2012. [CrossRef]

21. O'Driscoll, R.L.; Macaulay, G.J.; Gauthier, S.; Pinkerton, M.; Hanchet, S. Distribution, abundance and acoustic properties of Antarctic silverfish (*Pleuragramma antarcticum*) in the Ross Sea. *Deep Sea Res. Part II Top. Stud. Oceanogr.* **2011**, *58*, 181–195. [CrossRef]
22. Granata, A.; Cubeta, A.; Guglielmo, L.; Sidoti, O.; Greco, S.; Vacchi, M.; La Mesa, M. Ichthyoplankton abundance and distribution in the Ross Sea during 1987–1996. *Polar Biol.* **2002**, *25*, 187–202. [CrossRef]
23. Oozeki, Y.; Hu, F.; Kubota, H.; Sugisaki, H.; Kimura, R. Newly designed quantitative frame trawl for sampling larval and juvenile pelagic fish. *Fish. Sci.* **2004**, *70*, 223–232. [CrossRef]
24. Tamura, T.; Ohshima, K.I.; Fraser, A.D.; Williams, G.D. Sea ice production variability in Antarctic coastal polynyas. *J. Geophys. Res. Ocean.* **2016**, *121*, 2967–2979. [CrossRef]
25. Copernicus. Sea Ice. Available online: https://climate.copernicus.eu/sea-ice (accessed on 6 May 2023).